HiSST: 3rd International Conference on
High-Speed Vehicle Science Technology
14 -19 April 2024, Busan, Korea

# Numerical Study on the Characteristics of Detonation Wave Number in RDE

*Mohammed N. Nejaamtheen[1], Bu-Kyeng Sung[2] and Jeong-Yeol Choi[3]*

## Abstract

Detonation engines are likely to be integrated into various aerospace propulsion systems in the forthcoming era. Among the various types of detonation engines being investigated, the rotating detonation engine (RDE) stands out. Despite experimental explorations of the RDE, the intricate mechanism behind the propagation of rotating detonations remains inadequately understood. This work presents a comprehensive study focused on the wave dynamics along with key features of the detonation process and its effects on the flow-field. After reaching a quasi-steady state, the detonation structure in the azimuthal direction is investigated. The high temperature at the detonation front is determined to be around 2800~3100 K. The study investigates the influence of stagnation pressure ($p_0$) and stagnation temperature ($T_0$) on the detonation velocity ($U_D$). Lowering the $p_0$ results in decreased velocities, with the maximum velocity deficit ($U_{def}$) occurring at the lowest pressure value. Conversely, increasing $p_0$ leads to a more robust propagation of the detonation wavefront. Similar trends are observed for variations in $T_0$, indicating a weaker wavefront propagation with higher temperatures. The multi-probe study also reveals important details in the detonation front propagation region, the oblique shock wave region, and the combustor chamber exit. The study further explores the time-taken for wave stabilization, finding a correlation between wave number and the required stabilization time. The investigation of pressure peaks indicates an inverse relationship with the number of waves, suggesting significant dynamics influenced by the number of waves present. Beyond a certain threshold, an excessive number of waves can lead to detonation failure. The research findings reveal significant insights into the behavior of the RDE by shedding lights on the wave dynamics, and their implications for the performance and stability of RDE.

**Keywords**: *Rotating Detonation Engine (RDE), Detonation Wave number, Detonation speed, velocity deficit, stagnation pressure*

## Nomenclature

$U_D$ – detonation velocity
$U_{CJ}$ – Chapman-Jouguet velocity
$U_{def}$ – velocity deficit
$T_0$ – stagnation temperature
$T_1$ – initial temperature
$N_x$ – no. of grids along x-axis
$N_y$ – no. of grids along y-axis
$N_z$ – no. of grids along z-axis
$p_0$ – stagnation pressure
$h_{IG}$ – ignition zone height
$p_1$ – initial pressure
$d_0$ – outer-wall diameter
$h$ - channel width
*ms* – milli-seconds
$h$ – channel width
$t$ – computational time-step
$\Delta x$ – grid spacing along x-axis.
$\Delta y$ – grid spacing along y-axis.
$\Delta z$ – grid spacing along z-axis.
$t_s$ – stabilization time-step
$\delta t$ – time interval
$\omega$ – wave speed

[1] *Graduate Research Assistant, Pusan National University, Busan 46241, Republic of Korea*
[2] *Graduate Research Assistant, Pusan National University, Busan 46241, Republic of Korea*
[3] *Professor, Pusan National University, Busan 46241, Republic of Korea, aerochoi@pusan.ac.kr (Corresponding)*

## 1. Introduction

The Rotating Detonation Engine (RDE) stands at the forefront of cutting-edge propulsion technology, utilizing a sophisticated series of controlled explosions within a continuous power generation cycle to propel aircraft and spacecraft. With combustion velocities reaching astonishing speeds of thousands of meters per second, RDEs offer unparalleled efficiency and immense power potential. While the initial explorations of detonation applications in propulsion systems have laid the foundation [1], recent years have witnessed a surge in numerical [2-7] investigations, culminating in an extensive and up-to-date survey presented in references [8] and [9]. However, despite the substantial progress made thus far, our understanding of the intricate flow-field dynamics and complex detonation structures within three-dimensional (3D) RDEs remains limited. Previous studies have predominantly focused on two-dimensional (2D) RDE and 3D hydrogen-based configurations, leaving a critical knowledge gap regarding the behavior and performance of their higher hydrocarbon-based RDEs. It is imperative to address this gap and advance our comprehension of the fundamental principles underlying RDEs, as they hold great promise for the development of future propulsion systems.

In an exemplary display of circular RDE implementation, a meticulously designed and rigorously tested RDE, referred to as the PNU RPL-RDE, was examined at Pusan National University, Korea. With a focus on elucidating the characteristics of detonation propagation modes and assessing thrust performance under various operating conditions, an in-depth investigation was conducted, employing state-of-the-art high-speed camera imaging techniques to capture essential visual data. The comprehensive findings of this investigation have been documented and published [10] and [11]. Building upon the valuable insights garnered from the experimental study, the present research endeavors to expand upon the knowledge base by introducing a simplified version of the PNU RPL-RDE, and subsequently subjecting it to a comprehensive numerical investigation. By leveraging advanced computational techniques, this study aims to delve deeper into the intricate wave dynamics and the characteristics of the simplified RDE configuration.

This study focuses on Ethylene-based RDE. The primary focus of this investigation centers around analyzing the detonation wave-front characteristics and the stabilization time-taken for varying number of detonation waves inside the annular chamber after attaining a quasi-steady state. This study primarily aims to numerically investigate the 3D RDE and comprehensively understand the underlying unsteadiness of the flow-field during detonation propagation. By shedding light on these crucial aspects, we aspire to pave the way for the realization of practical and efficient RDE designs, ultimately propelling the field of aerospace propulsion into a new era of performance and efficiency.

## 2. Numerical Methodology

An internally developed in-house solver has been implemented to effectively calculate the chemical source terms. The comprehensive formulation of an unsteady and compressible Navier-Stokes equations, represented by Equation (1) and Equation (2), encapsulates the essential mathematical expressions required to accurately model and simulate the intricate flow behavior.

$$\frac{\partial Q}{\partial t}+\frac{\partial E}{\partial x}+\frac{\partial F}{\partial y}+\frac{\partial G}{\partial z}=\frac{\partial E_v}{\partial x}+\frac{\partial F_v}{\partial y}+\frac{\partial G_v}{\partial z}+W \qquad (1)$$

$$Q=\begin{bmatrix}\rho_i\\ \rho u\\ \rho v\\ \rho w\\ e\\ \rho k\\ \rho\omega\end{bmatrix} E=\begin{bmatrix}\rho_i u\\ \rho u^2+p\\ \rho vu\\ \rho wu\\ (e+p)u\\ \rho uk\\ \rho u\omega\end{bmatrix} F=\begin{bmatrix}\rho_i v\\ \rho vu\\ \rho v^2+p\\ \rho wv\\ (e+p)v\\ \rho vk\\ \rho v\omega\end{bmatrix} G=\begin{bmatrix}\rho_i w\\ \rho wu\\ \rho wv\\ \rho w^2+p\\ (e+p)w\\ \rho wk\\ \rho w\omega\end{bmatrix} E_v=\begin{bmatrix}-\rho_i u_i^d\\ \tau_{xx}\\ \tau_{xy}\\ \tau_{xz}\\ \beta_x\\ \mu_k\,\partial k/\partial x\\ \mu_\omega\,\partial\omega/\partial x\end{bmatrix} F_v=\begin{bmatrix}-\rho_i v_i^d\\ \tau_{yx}\\ \tau_{yy}\\ \tau_{yz}\\ \beta_y\\ \mu_k\,\partial k/\partial y\\ \mu_\omega\,\partial\omega/\partial y\end{bmatrix} G_v=$$

$$\begin{bmatrix}-\rho_i w_i^d\\ \tau_{zx}\\ \tau_{zy}\\ \tau_{zz}\\ \beta_z\\ \mu_k\,\partial k/\partial z\\ \mu_\omega\,\partial\omega/\partial z\end{bmatrix} w=\begin{bmatrix}w_i\\ 0\\ 0\\ 0\\ 0\\ s_k\\ s_\omega\end{bmatrix} \quad (2)$$

To ensure numerical stability, the approach employs fixed time intervals, aiming to keep the maximum Courant-Friedrichs-Lewy (CFL) number below 0.5. To facilitate parallel execution, OpenMP is employed to distribute the computational workload of the chemical source terms evenly across multiple processors. Spatial discretization is achieved using a third-order Weighted Essentially Non-Oscillatory (WENO) scheme, while temporal discretization is implemented using a second-order implicit Runge-Kutta method.

Convective fluxes are discretized utilizing the robust and precise AUSMDV (Advection Upwind Splitting Method flux Difference and Vector splitting biased) flux-splitting scheme. In terms of the chemistry model, a quasi-globally reduced reaction mechanism comprising 9 species and 10 reaction steps is chosen. For further detailed insights into the numerical scheme and solver methodology, interested readers are encouraged to refer to previous works [6, 7], which provide comprehensive explanations of the computational approach and solution techniques employed.

## 3. Computational Domain

A simplified representation of a rotating detonation combustor is constructed using an annular confinement equipped with inlet and outlet ports. Fig 1. depicts the pressure contour revealing the distinct advancement of the detonation wave in a steady and stabilized manner. The $d_0$ of the channel measures 25 mm, while the $h$ is 4.5 mm. Furthermore, the channel extends to a length of 100 mm. The initial state of the combustor involves introducing cold air at the inlet with a specified temperature ($T_1$) and pressure ($p_1$). To initiate the detonation wave, a one-dimensional (1D) steady Zeldovich–von Neumann–Döring (ZND) structure solution is superimposed onto a subsection of the domain adjacent to the inlet surface. To stabilize the tail of the ignition zone, the high pressure and temperature in the post-shock area are appropriately filtered. The inflow boundary is characterized by periodic pressure conditions, while the outflow boundary is determined by characteristic conditions. The sidewalls, on the other hand, are modeled as slip conditions.

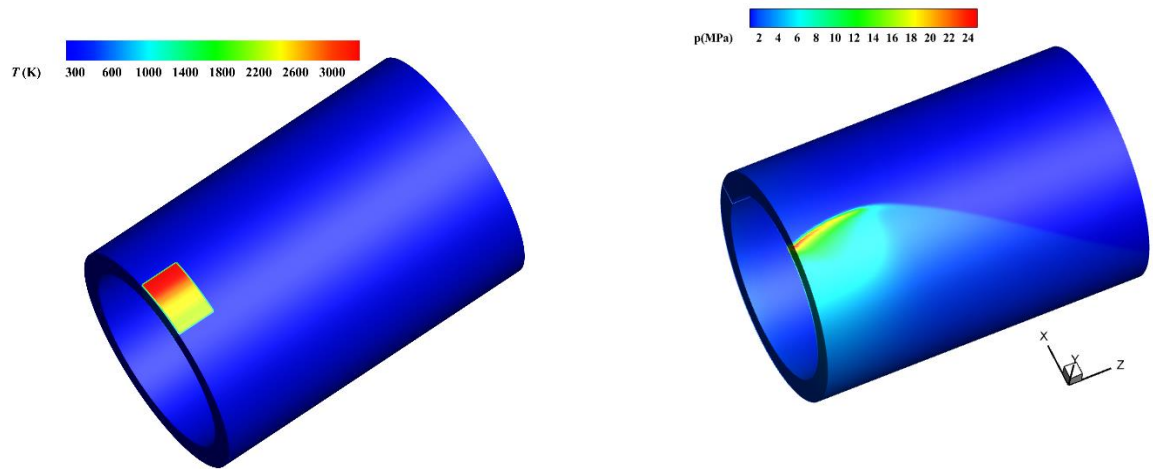

**Fig 1.** (a) A schematic of the combustor geometry with superimposed initial conditions of temperature and (b) pressure contour revealing the propagation of the detonation.

**Table. 1 Comprehensive overview of the mesh specifications.**

| Name | $N_x$ x $N_y$ x $N_z$ | $\Delta x$ | $\Delta y$ | $\Delta z$ | Grid size |
|---|---|---|---|---|---|
| Grid1 | 393 x 6 x 189 | 0.01 | 0.01 | 0.01 | 445,662 |
| Grid2 | 471 x 10 x 189 | 0.01 | 0.01 | 0.01 | 890,190 |
| Grid3 | 521 x 13 x 189 | 0.009 | 0.009 | 0.009 | 1,280,097 |
| Grid4 | 571 x 16 x 189 | 0.009 | 0.009 | 0.009 | 1,726,704 |
| Grid5 | 601 x 20 x 189 | 0.008 | 0.008 | 0.008 | 2,271,780 |

Throughout the study, structured orthogonal meshes have been utilized. A comprehensive summary of all the meshes employed in this investigation is provided in Table I. A thorough grid refinement study has been conducted, resulting in the selection of an optimal resolution. Our simulations utilizing Grid3 and higher resolutions yielded very similar results, with a low error percentage. Consequently, for the sake of efficiency and to establish a consistent benchmark, we have chosen Grid3 as the baseline configuration for all subsequent simulations.

## 4. Results and Discussions

### 4.1. Preliminary study

Utilizing the acquired baseline conditions and grid resolution, an initial investigation was conducted to gain insight. Since the primary focus of this comprehensive study revolves around examining the wave dynamics characteristics following the attainment of a quasi-stable state, the plot presented in Figure 2 plays a crucial role in pinpointing the precise time step at which the quasi-steady condition is established. The results, demonstrated in Figure 2, exhibit the recorded inlet and exit Mach numbers obtained from a probe randomly positioned at both locations. After an initial period of fluctuation, stability is reached at 0.168 ms, serving as the reference time step for all subsequent analyses.

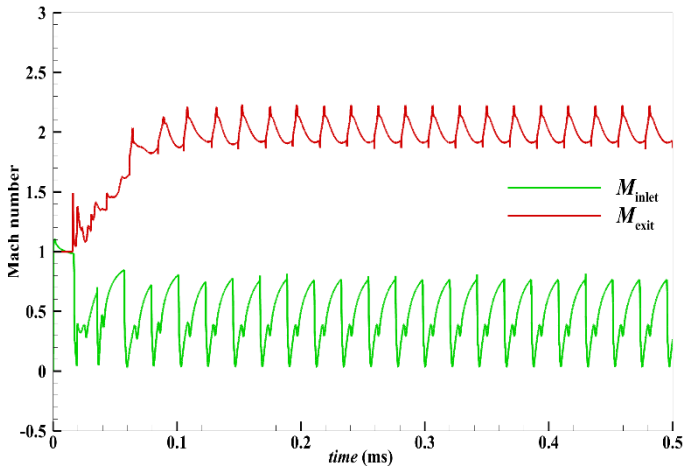


**Fig 2.** Mach number readings demonstrate stable propagation at both the inlet and exit planes after 0.168ms

To provide additional support for the results shown in Fig. 2, Fig. 3 displays the contours of temperature at various time instances. Following the initialization phase, a small, reversed detonation wave emerges from the initial collision between the primary detonation wave and the trailing edge of the ignition zone

at t = 0.50ms. Its height rapidly increases until it collides with the main detonation wave at t = 0.102ms. Subsequent collisions between the rotating waves lead to the sustenance of a single rotating wave stabilization at ts = 0.168ms within the combustor annulus, characterized by varying fill heights compared to the initial ignition zone height. It is important to note that this process exhibits distinct behavior in the radial and azimuthal directions, particularly when multiple detonation waves propagate. Further analysis of this phenomenon will be discussed in subsequent sections.

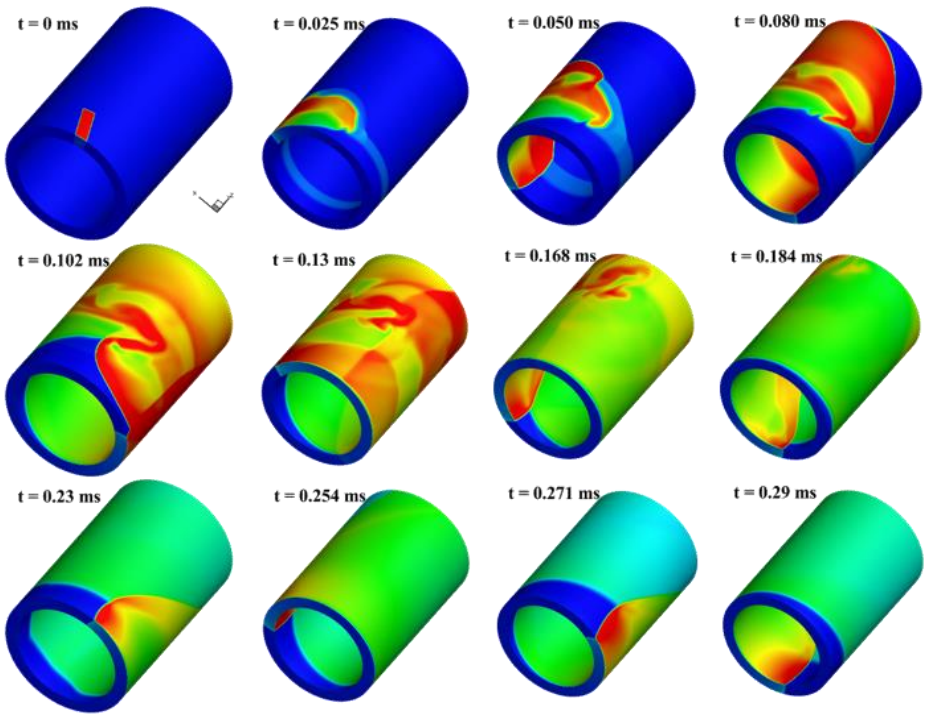


**Fig 3.** Instantaneous temperature contours at different time intervals.

### 4.2. Characteristics of Detonation Waves

This section provides a brief discussion of the characteristics of the detonation wave, focusing on $p_0$, and $T_0$. Fig. 4(a) illustrates the variation of the $U_D$ relative to the Chapman-Jouguet velocity ($U_{CJ}$) under different $p_0$ conditions. The results indicate that both the $U_D$ and $U_{CJ}$ decrease as $p_0$ decreases implying that lower $p_0$ results in reduced UD compared to the ideal $U_{CJ}$. Notably, the lowest $p_0$ value also exhibits the largest $U_{def}$, indicating a significant deviation from the expected $U_{CJ}$. Conversely, as the $p_0$ increases, the pressure peak associated with the detonation wave also increases indicating a more robust propagation of the detonation wavefront. The higher-pressure peak signifies enhanced combustion performance and more efficient energy release within the wave. These findings highlight the significant influence of stagnation pressure on the characteristics of the detonation wave, affecting both its velocity and pressure behavior.

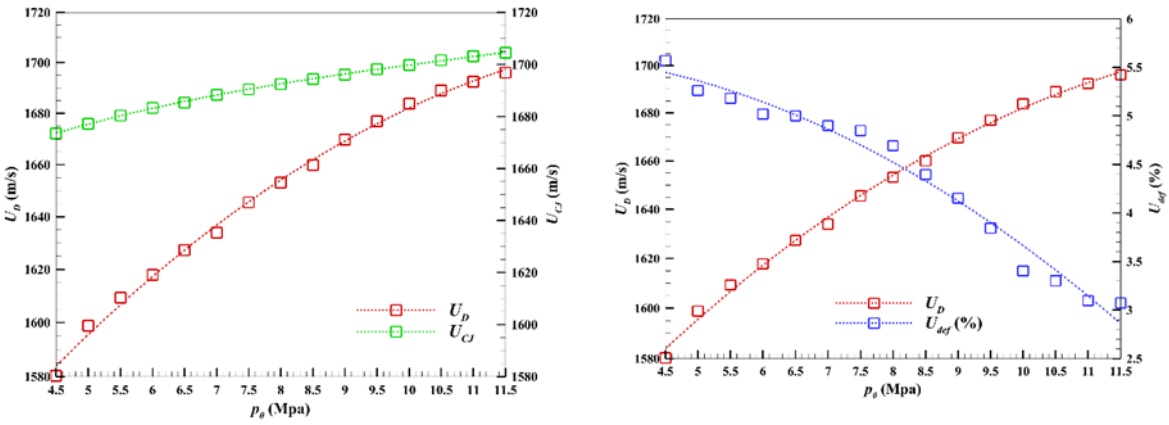


**Fig 4.** The impact of varying $p_0$ on $U_D$ comparing with (a) $U_{CJ}$ and (b) $U_{def}$

For a more in-depth analysis of the detonation wave characteristics, the mid-plane of the annular chamber is visualized in an unwrapped format, as depicted in Fig. 5, where the instantaneous pressure contour is superimposed with the relevant nomenclature for clarity and reference.

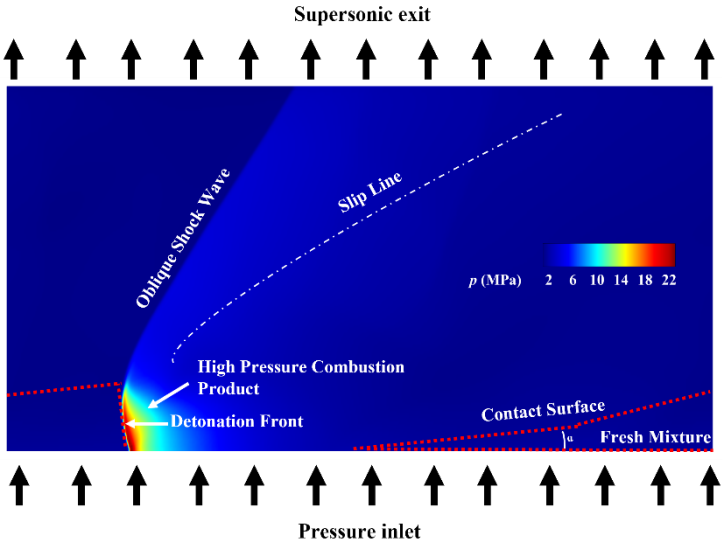


**Fig 5.** The instantaneous pressure contour of the unwrapped annular chamber highlights the crucial nomenclature associated with the detonation wave.

To measure pressure and monitor the $U_D$, a numerical pressure probe is positioned near the inlet surface at a location corresponding to 3% of the chamber height ($h_c$). Figure 6(a) depicts the normalized pressure profile obtained from this probe, and the unwrapped results are presented for a range of stagnation pressures, spanning from 4.5 MPa to 11 MPa. Notably, the normalized pressure profile appears nearly identical ahead of the shock, indicating that changes in $p_0$ have minimal influence on the pre-shock conditions. In contrast, as observed in Fig. 6(b), the normalized pressure profile exhibits an upward trend with increasing $T_0$, indicating a positive correlation between variations in $T_0$ and the pre-shock condition. This suggests that the pre-shock condition is inversely proportional to $T_0$.

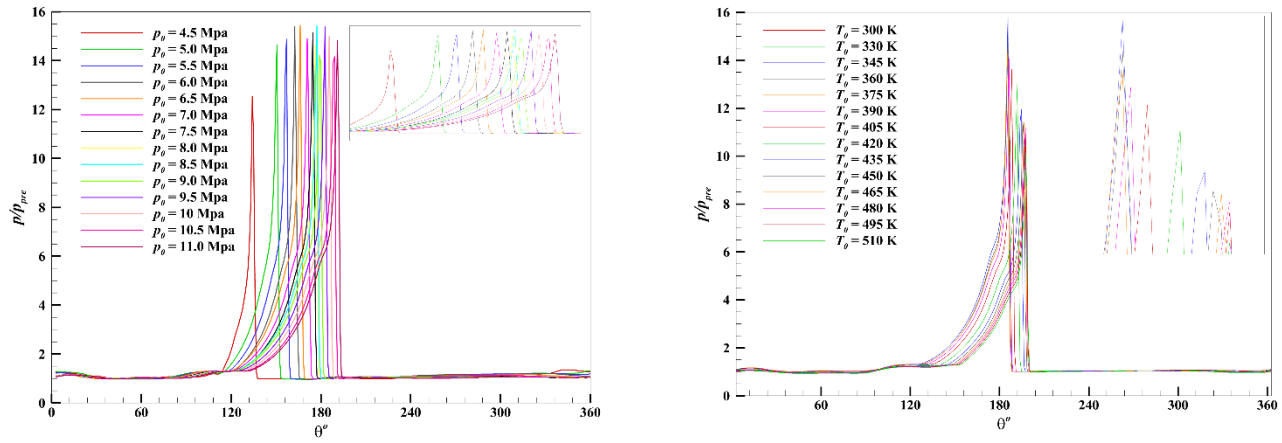


**Fig 6.** Normalized pressure near the inlet of an unwrapped domain for (a) varying $p_0$ and (b) varying $T_0$.

### 4.3. Multiplicity of Detonation Waves

This section explores the study of wave dynamics characteristics in the presence of multiple waves by introducing multiple ignition regions that are evenly distributed. Each ignition location is subjected to identical thermo-physical parameters, thereby establishing a mode-locked condition as described in Ref. [14]. At specific time instances, Fig. 7 presents the instantaneous temperature contours acquired multiple detonation wave propagation using the baseline condition of $p_0$ = 1.7MPa and $T_0$ = 360K.

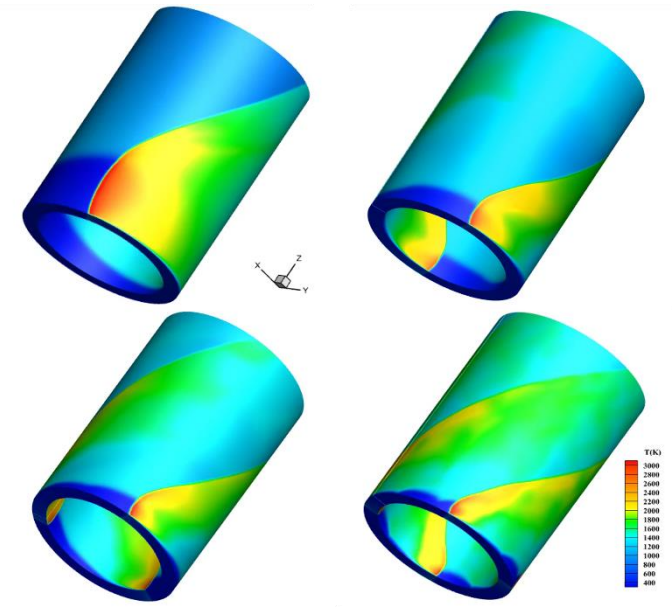


**Fig 7.** Instantaneous temperature contours obtained at $p_0$ = 1.7MPa and $T_0$ = 360K at a specific time intervals showing (a) one wave, (b) two wave, (c) three wave, and (d) four wave

Fig.8 showcases the relative error derived from the time-dependent evolution of the pressure contour using two different methods: (a) the normal line segment method and (b) the Stineman interpolation method. The calculations are performed at $p_0$ = 1.7MPa and $T_0$ = 360K for four distinct wave number conditions, each initialized with evenly distributed ignition zones. The table 2 below presents the stabilization times (ts) for various wave conditions. Each wave condition is characterized by the number of waves present in the system. The number of stable detonation waves corresponds to the number of

ignition regions employed. The ts is represented as a percentage of the total time duration, with one-wave stabilizing at 25.9%, two-wave at 38.0%, three-wave at 53.9%, and four-wave at 76.1%. This demonstrates the impact of the number of waves on the time required for stabilization. Notably, as the number of waves increases, a noticeable reduction in the fill height is also observed. This trend persists for up to five ignition zones. However, it is important to note that further increasing the number of initial zones in the domain ultimately leads to detonation failure.

**Table. 2 Stabilization Times for Different Wave Conditions**

| Wave number | Stabilization time |
|---|---|
| 1 | 25.9% |
| 2 | 38.0% |
| 3 | 53.9% |
| 4 | 76.1% |

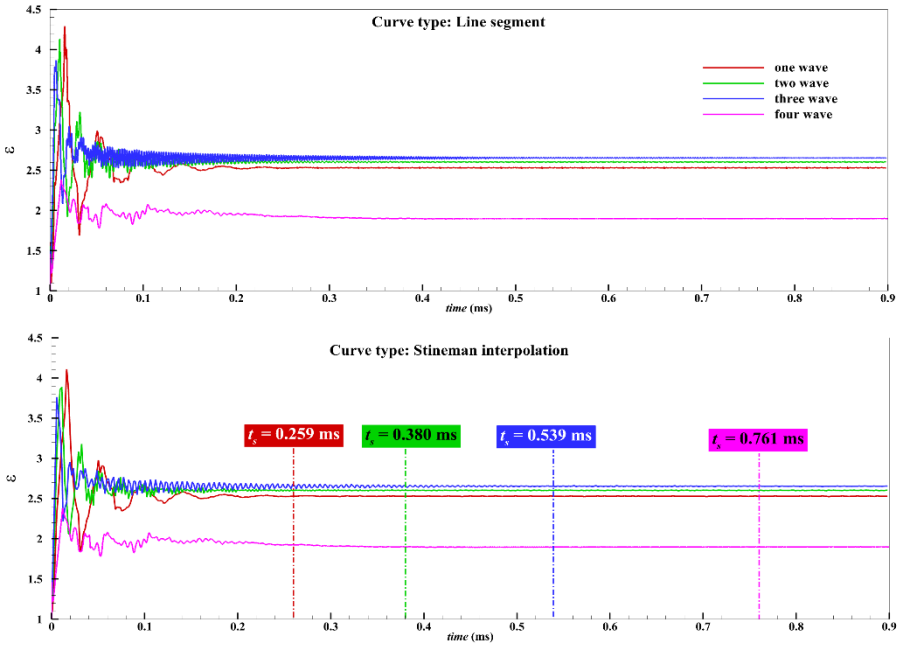


**Fig 8.** The relative error, obtained from the time-dependent evolution of the pressure for two different methods: (a) normal line segment method and (b) Stineman interpolation method.

The relationship between the $t_s$, time interval ($\delta t$), and $U_D$, as a function of wave number ($\omega$), is depicted in Fig. 9. It is observed that the $\delta t$ and $t_s$ for wave stabilization exhibit a direct correlation with the $\omega$. As the $\omega$ increases, the $\delta t$ experiences a significant decrease of approximately 40% to 50%. This decrease is directly associated with the $U_D$, indicating that an increase in detonation velocity leads to a reduction in both the $\delta t$ and $t_s$. Consequently, the margin between the $U_D$ and $U_{CJ}$ also expands as the

$\omega$ increases showing a clear relationship between the $U_D$, $\delta t$, and $t_s$ in the context of multiple detonation waves.

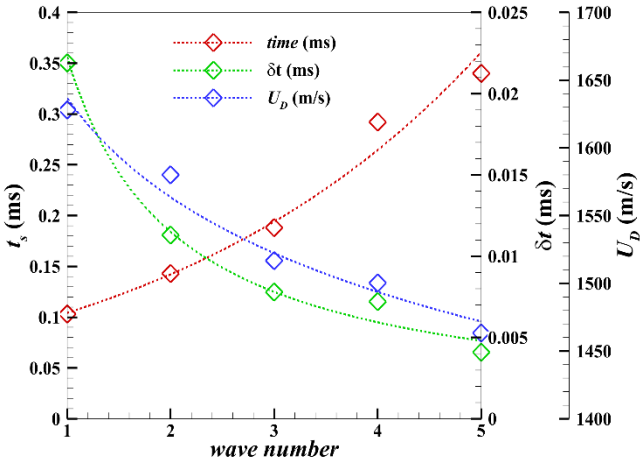


**Fig 9.** The relative error, obtained from the time-dependent evolution of the pressure for two different methods: (a) normal line segment method and (b) Stineman interpolation method.

### 4.4. Conclusion

This study presents a comprehensive examination of wave dynamics, key detonation features, and their impact on the flow field. The analysis focuses on the azimuthal detonation structure after attaining a quasi-steady state. The investigation reveals that the temperature at the detonation front reaches approximately 2800~3100 K. The influence of $p_0$ and $T_0$ on the detonation wave velocities are examined. Decreasing $p_0$ results in lower velocities, with the maximum $U_{def}$ observed at the lowest pressure level. Conversely, increasing $p_0$ enhances the robustness of the detonation wavefront propagation. Similar trends are observed with variations in $T_0$, indicating weaker wavefront propagation at higher temperatures. The study utilizes multi-probe measurements to gain insights into the propagation regions of the detonation front, oblique shock waves, and the combustor chamber exit. Additionally, the investigation explores the time required for wave stabilization, finding a correlation between the number of waves and the stabilization time. The analysis of pressure peaks reveals an inverse relationship with the number of waves, indicating significant dynamics influenced by the presence of multiple waves. However, an excessive number of waves can lead to detonation failure beyond a certain threshold. Overall, this research provides valuable insights into the behavior of the RDE, shedding light on wave dynamics and their implications for the performance and stability of the rotating detonation engine. The findings contribute to the advancement of knowledge in this field, paving the way for further exploration and optimization of RDE technology in aerospace propulsion systems.

## References

1. Nicholls, J. A., and Cullen, R. E., "The feasibility of a rotating detonation wave rocket motor," MICHIGAN UNIV ANN ARBOR, 1963.
2. Pan, Z., Fan, B., Zhang, X., Gui, M., & Dong, G., "Wavelet pattern and self-sustained mechanism of gaseous detonation rotating in a coaxial cylinder," Combustion and Flame, Vol. 158, No. 11, 2011, pp. 2220, 2228. doi: 10.1016/j.combustflame.2011.03.016
3. Yi, T. H., Lou, J., Turangan, C., Choi, J. Y., and Wolanski, P., "Propulsive performance of a continuously rotating detonation engine," Journal of Propulsion and Power, Vol. 27, No. 1, 2011, pp. 171, 181. doi: 10.2514/1.46686

4. Uemura, Y., Hayashi, A. K., Asahara, M., Tsuboi, N., and Yamada, E., "Transverse wave generation mechanism in rotating detonation," Proceedings of the Combustion Institute, Vol. 34, No. 2, 2013, pp. 1981, 1989. doi: 10.1016/j.proci.2012.06.184
5. Niyasdeen, M., Oh, S., Kim, K. S., and Choi, J. Y., "Quasi-steady state simulation of rotating detonation engine," International Journal of Aeronautical and Space Sciences, Vol. 16, No. 4, 2015, pp. 548, 559. doi: 10.5139/ijass.2015.16.4.548
6. Zhang, P., Meagher, P. A., and Zhao, X., "Multiplicity for idealized rotational detonation waves," Physics of Fluids, Vol. 33, No. 10, 2021, pp. 106102. doi: 10.1063/5.0063837
7. Nejaamtheen, M. N., Kim, T. Y., Pavalavanni, P. K., Ryu, J., and Choi, J. Y., "Effects of the dimensionless radius of an annulus on the detonation propagation characteristics in circular and non-circular rotating detonation engines," Shock Waves, Vol. 31, No. 7, 2021, pp. 703, 715. doi: 10.1007/s00193-021-01065-z
8. Xie, Q., Ji, Z., Wen, H., Ren, Z., Wolanski, P., and Wang, B., "Review on the Rotating Detonation Engine and It's Typical Problems," Transactions on Aerospace Research, Vol. 2020, No. 4, 2020, pp. 107, 163. doi: 10.2478/tar-2020-0024
9. Raman, V., Prakash, S., and Gamba, M., "Nonidealities in Rotating Detonation Engines," Annual Review of Fluid Mechanics, Vol. 55, No. 1, 2023, pp. 639, 674. doi: 10.1146/annurev-fluid-120720-032612
10. Lee, J. H., Ryu, J. H., Lee, E. S., Han, H. S., Choi, J. Y.: Experimental Proof of Concept of a Noncircular Rotating Detonation Engine (RDE) for Propulsion Applications. Aerospace (2022). http://doi: 10.3390/aerospace10010027
11. Han, H. S., Lee, E. S., Choi, J. Y.: Experimental Investigation of Detonation Propagation Modes and Thrust Performance in a Small Rotating Detonation Engine Using C2H4/O2 Propellant. Energies (2021). http://doi: 10.3390/en14051381
12. Choi, J. Y., Kim, D. W., Jeung, I. S., Yang, V.: Cell-like structure of unstable oblique detonation wave from high-resolution numerical simulation. Proc. of the Comb. Inst. (2007). http://doi: 10.1016/j.proci.2006.07.173
13. Jeong, S. M., Lee, J. H., Choi, J. Y.: Numerical investigation of low-frequency instability and frequency shifting in a scramjet combustor. Proc. of the Comb. Inst. (2022). http://doi: 10.1016/j.proci.2022.07.245
14. Koch, J., Kurosaka, M., Knowlen, C., Kutz, J. N.: Mode-locked rotating detonation waves: Experiments and a model equation. Physical Review E (2020). doi: 10.1103/physreve.101.013106

 